DESIGN DUAL-MODE BANDPASS FILTERS BASED ON SYMMETRICAL T-SHAPED STUB-LOADED STEPPED-IMPEDANCE RESONATORS WITH HIGH FREQUENCIES SELECTIVITY

Changhai Hu[1], Xiangzheng Xiong[1], Yanliang Wu[2, *], and Cheng Liao[1]

[1]Institute of Electromagnetic Field and Microwave Technology, Southwest Jiaotong University, Chengdu 610031, China

[2]Department of Computer and Communication Engineering, Emei Campus, Southwest Jiaotong University, Emeishan 614202, China

Abstract—A novel approach for designing planar dual-mode bandpass filters using symmetrical T-shaped stub-loaded stepped-impedance resonators (TSLSIRs) with high frequencies selectivity is presented. The proposed symmetrical TSLSIR structure is mainly composed of three elements, i.e., a stepped-impedance resonator (SIR), and two T-shaped stubs which symmetrically loaded at the middle sections of the SIR. Two dual-mode bandpass filters based on TSLSIRs with high frequency selectivity are proposed for experimental verification. Firstly, a dual-mode single passband filter with two transmission zeros located at the both sides of passband is presented, whose passband is centered at 5.23 GHz with the fractional bandwidth of 10.1%, and a wide upper-stopband with harmonic suppression better than 20 dB in the range of 5.9 GHz to 12.9 GHz is achieved. Secondly, a dual-mode dual-band bandpass filter with four transmission zeros located at the both sides of the two passbands is presented, whose two passbands are centered at 3.4 GHz and 4.54 GHz with the corresponding fractional bandwidth of 8.4% and 7.5% respectively, and the spurious frequencies from 4.9 GHz to 8.45 GHz are successfully suppressed to the level of lower than −20 dB. Both filters have been designed, fabricated and measured. The measured results show good agreements with those of the simulation.

1. INTRODUCTION

With the rapid development of wireless communication technology, the planar microwave filters with good frequency selectivity, compact size, and wide stopband have attracted much attention in recent years [1, 2]. Especially, the high-performance dual-mode bandpass filters have become attractive components [3–8] since they can provide several advantages over other conventional bandpass filters [9, 10], such as high frequency selectivity, good passband performances, and compact size. The primary planar microwave dual-mode filter was presented by Wolff [11]. Since then a lot of researchers have been investigating various dual-mode microstrip resonator structures. The typical dual-mode microstrip resonators are based on geometric symmetry structures with perturbation elements at the symmetry plane, such as ring resonator [12], square-ring resonator [13], multi-arc resonators [14], and open-loop stub-loaded resonators [15] etc.. On the other hand, the dual-mode dual-band bandpass filters have received increasing attentions [16–21] because they have the advantages of good passband characteristics and compactness over other conventional dual-band bandpass filters. However, it is still a challenge to design single or dual passband dual-mode filters with sharp frequency selectivity.

In this work, a novel approach of the design of dual-mode single and dual passband bandpass filters based on symmetrical TSLSIRs with good frequency selectivity is proposed. Then two prototype filters have been designed and fabricated for experimental verification. By introducing source-load cross-coupling structure, additional finite-frequency transmission zeros can be generated near each edge of passband to improve the frequency selectivity and out-of-band harmonic suppression. It may be seen that the proposed dual-mode single-band bandpass filter exhibits two transmission zeros which are located close to the passband edges, and the proposed dual-mode dual-band bandpass filter has four transmission zeros whose locations are very close to the two passband edges to increase frequency selectivity. Both filters have been simulated and measured. The measurement results show good agreements with those of the coupling matrix analysis and electromagnetic simulation.

2. DUAL-MODE SINGLE-BAND BANDPASS FILTER

Figure 1(a) shows the layout of the proposed filter whose passband is centered at 5.23 GHz with the fractional bandwidth of 10.1%. The proposed filter consists of symmetrical TSLSIR and the capacitive source-load cross-coupling structure. The corresponding coupling

scheme is shown in Figure 1(b) and the source is coupled to both modes, represented by the solid lines, and so is the load. There is no coupling between the two modes. Furthermore, the source and load are also coupled through the weak-coupling path which is denoted by the dash line in Figure 1(b). The proposed filter is fabricated on the Rogers RT/Duroid5880 substrate with dielectric constant ratio ε_r of 2.2 and thickness h of 0.508 mm. The structure dimensions of this filter are given in Table 1.

Table 1. Dimensions of the proposed filter.

Parameters	Values	Parameters	Values	Parameters	Values
W_{t1}	0.35	W_4	1.4	L_3	0.41
W_{t2}	0.25	L_{t0}	3.3	L_4	2.18
W_0	1.54	L_{t1}	3.19	L_5	0.85
W_1	0.24	L_{t2}	3.73	S_1	0.2
W_2	0.27	L_1	7.24	S_2	0.59
W_3	4.51	L_2	2.93	D_1	0.6
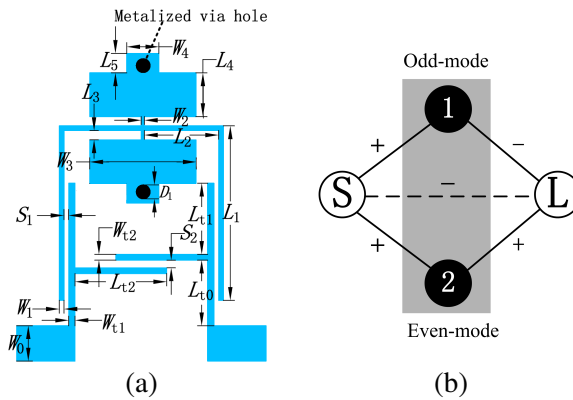
Figure 1. (a) Layout of proposed dual-mode single-band bandpass filter. (b) Corresponding coupling scheme (1 and 2 represent the odd and even modes, respectively).

2.1. Analysis of Dual-mode Symmetrical TSLSIR with Short-circuited Loaded Case

The proposed dual-mode symmetrical TSLSIR with short-circuited loaded case is illustrated in Figure 2(a). Because the dual-mode resonator is symmetrical about the A-A' plane, the odd- and even-mode theory may be employed to analyze it [15, 22]. Under the
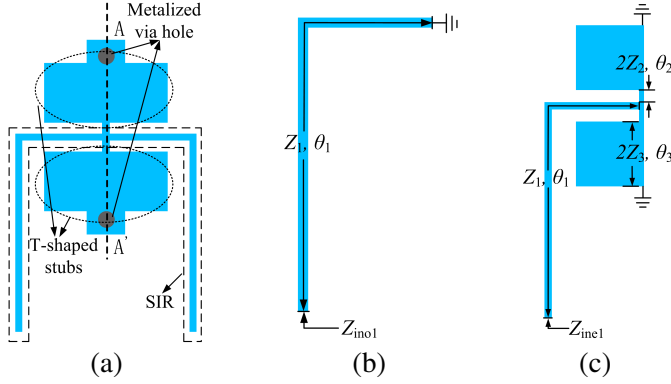
Figure 2. (a) Configuration of TSLSIR with short-circuited loaded case. (b) Odd mode equivalent circuits of TSLSIR. (c) Even-mode equivalent circuits of TSLSIR.

odd- and even-mode excitations, the dash line in Figure 2(a) may be considered as a perfect magnetic wall and electric wall. In Figures 2(b) and (c), where Z_{ino} and Z_{ine} are the input impedances of odd- and even-mode resonances respectively. Z_i is the characteristic impedance and θ_i is the electrical length ($i = 1, 2, 3$).

Ignoring the impact of step discontinuity and open-edge capacitance, the odd mode equivalent circuit of TSLSIR with short-circuited loaded case is shown in Figure 2(b), and the input impedance may be given as follow:

$$Z_{\mathrm{ino1}} = jZ_1 \tan \theta_1 \qquad (1)$$

Theoretically, the resonance condition of odd mode is $Z_{\mathrm{ino1}} = \infty$ then the odd mode resonant frequency may be expressed as:

$$f_{\mathrm{odd1}} = \frac{(2n-1)c}{4(L_1 + L_2)\sqrt{\varepsilon_{\mathit{eff}}}} \qquad (2)$$

where $n = 1, 2, 3, \ldots$, c is the speed of light in free space, $\varepsilon_{\mathit{eff}}$ the equivalent dielectric constant, and L_1 and L_2 are the parameters which shown in Figure 1(a). From Eq. (2), it may be observed that the odd mode resonant frequency only depends on the L_1 and L_2.

The even-mode equivalent circuit of TSLSIR with short-circuited loaded case is shown in Figure 2(c), the even-mode resonance occurs when $Z_{\mathrm{ine1}} = \infty$ and the input impedance may be expressed as:

$$Z_{\mathrm{ine1}} = jZ_1 \frac{C + Z_1 \tan \theta_1 \cdot D}{Z_1 \cdot D - \tan \theta_1 \cdot C} \qquad (3)$$

where $C = Z_2(Z_2 \tan \theta_2 + Z_3 \tan \theta_3)$ and $D = Z_2 - Z_3 \tan \theta_2 \tan \theta_3$.

From Eq. (3), it may be found that the even-mode resonant frequency depends on the Z_1, Z_2, Z_3, θ_1, θ_2 and θ_3.

Substituting the parameter values of the proposed filter into the Eqs. (1), (2) and (3) and solving them with MATLAB program, the resonant frequencies may be obtained. The calculated resonant frequencies with different width parameters are shown in Figures 3(a) and (b). The horizontal axis is the width in mm, the vertical axis is the resonant frequency. As shown in Figure 3(a), when W_1, W_2, W_3 varies from 0.1 mm to 5 mm respectively, the corresponding even-mode resonant frequencies change as following three cases: almost keeping the same, only increasing a little and increasing a lot. The Figure 3(b) shows the calculated resonant frequencies vary with the length parameters. It may be seen that when L_2, L_3 and L_4 increase
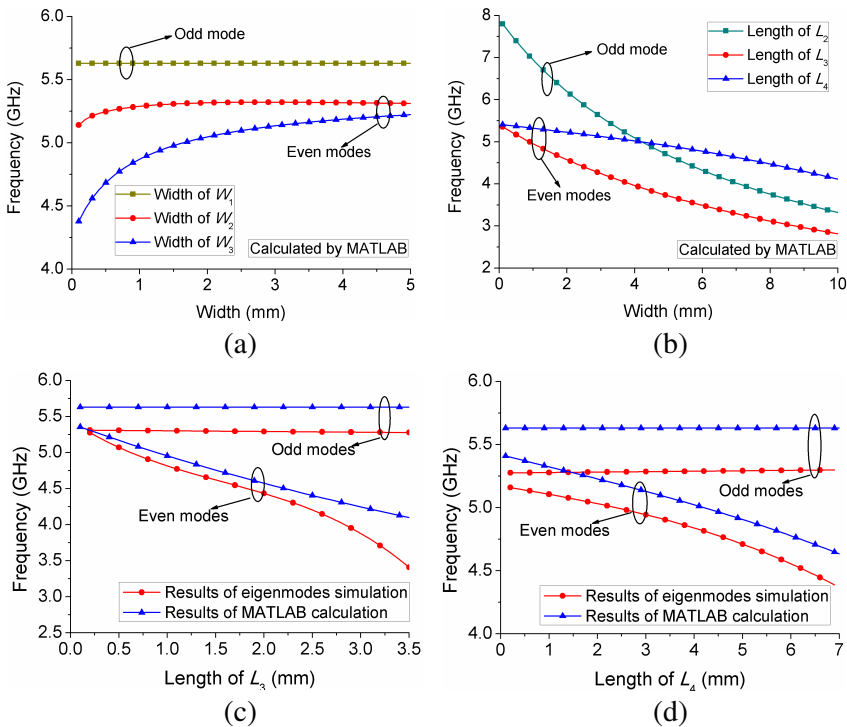
Figure 3. (a) The calculated resonant frequencies vary with width parameters. (b) The calculated resonant frequencies vary with length parameters. (c) The comparison between eigenmodes simulation and MATLAB calculation with different L_3. (d) The comparison between eigenmodes simulation and MATLAB calculation with different L_4.

from 0.1 mm to 10 mm respectively, the odd- and even-mode resonant frequencies decrease almost linearly and adjusting the parameter of L_3 may obtain faster dropping rate of the even-mode frequency. Moreover when the value of L_2 is the practical fabrication dimension, i.e., 2.93 mm, the relative frequency deviation between calculating frequency (5.63 GHz) and the measured center frequency (5.22 GHz) is 7.9%. Figure 3(c) shows the comparison between the results of eigenmodes simulation and the results of MATLAB calculation with different L_3. It can be seen that when L_3 varies from 0.2 mm to 3.5 mm the resonant frequencies of the even mode decrease almost linearly and meanwhile the resonant frequencies of the odd mode is almost constant. Moreover, the relative frequency deviation between the calculated odd mode frequency and the odd mode frequency of eigenmodes simulation is 6.2% and the most of the frequency relative deviations between the two even-mode curves in Figure 3(c) is around 3.2%. Figure 3(d) shows the comparison between the results of eigenmodes simulation and the results of MATLAB calculation with different L_4. As illustrated in Figure 3(d), when L_4 varies from 0.1 mm to 7 mm, the even-mode resonant frequencies decrease almost linearly, but the resonant frequency of the odd mode is almost constant. The relative frequency deviation between the two even-mode curves in Figure 3(d) is about 4% and the relative frequency deviation between the two odd mode curves is about 6.4%. As illustrated in Figures 3(c) and (d), the common characteristics may be found as follows: when the L_3 and L_4 increase, the even-mode frequency moves towards the lower frequency, whereas the odd mode frequency remains stationary. In short, it can be seen that the results of MATLAB calculation well agree with the results of eigenmodes simulation, in other words the Eqs. (1), (2) and (3) and the equivalent circuits proposed in Figures 2(b) and (c) have been well convinced.

2.2. Dual-mode Single-band Bandpass Filter Design

Figures 4(a) and (b) show the mode distribution with different lengths of L_3 and L_4, respectively. In Figure 4(a), the even-mode frequency moves towards the lower frequency when L_3 increases, whereas the odd mode frequency remains stationary. The same is true for Figure 4(b). It can be seen that the odd mode resonant frequency is scarcely affected by the lengths of L_3 and L_4, and the even-mode resonant frequency can be conveniently adjusted by changing the lengths of L_3 and L_4.

Furthermore, with the coupling scheme in Figure 1(b), the
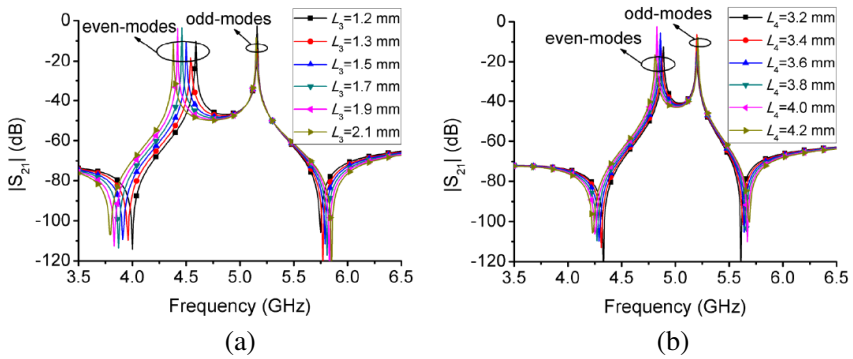
Figure 4. (a) Simulated $|S_{21}|$ in dB with the varied L_3. (b) Simulated $|S_{21}|$ in dB with the varied L_4.

corresponding coupling matrix M can be expressed as [23]:

$$M = \begin{bmatrix} 0 & M_{S1} & M_{S2} & M_{SL} \\ M_{S1} & M_{11} & 0 & M_{1L} \\ M_{S2} & 0 & M_{22} & M_{2L} \\ M_{SL} & M_{1L} & M_{2L} & 0 \end{bmatrix} \quad (4)$$

Since the proposed dual-mode filter exhibits symmetry, the relationship among the coupling matrices presents $M_{S1} = -M_{1L}$ and $M_{S2} = M_{2L}$, and the coupling between the two modes is 0. Furthermore, as the proposed S-L coupling structure is a capacitive coupling, the S-L coupling coefficient $M_{SL} < 0$. According to the analysis above, the corresponding coupling coefficients [24–26] can be synthesized as:

$$M = \begin{bmatrix} 0 & 0.9067 & 0.9142 & -0.0390 \\ 0.9067 & -1.8475 & 0 & -0.9067 \\ 0.9142 & 0 & 1.8235 & 0.9142 \\ -0.0390 & -0.9067 & 0.9142 & 0 \end{bmatrix} \quad (5)$$

The normalized frequency response of the proposed filter under the coupling matrix in the Eq. (5) is shown in Figure 5(a). For visual comparison with the electromagnetic simulated results, the frequency response curves of simulation and coupling matrix are combined, as shown in Figure 5(b). It can be seen that the simulated results show good agreements with those of theoretical coupling matrix analysis.

As shown in Figure 5(b), the simulated 3 dB passband is centered at 5.23 GHz with the corresponding fractional bandwidth of 10.1%, and the in-band return loss is less than -20 dB. Meanwhile, a wide upper-stopband with harmonic suppression better than 20 dB in the range
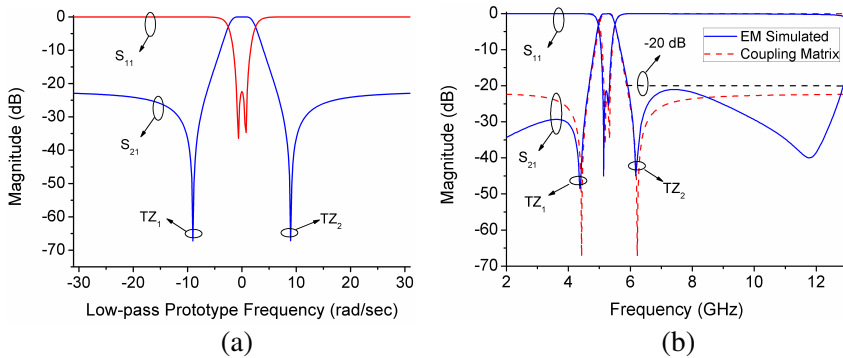
Figure 5. (a) Low-pass prototype frequency responses from coupling matrix. (b) Comparison of frequency response curves of the proposed filter.
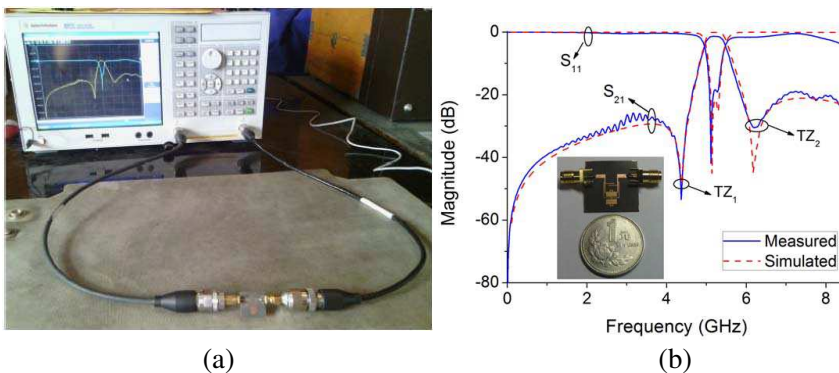
Figure 6. (a) The photograph of measured environment. (b) Simulation and measurement results with photograph of fabricated filter.

of 5.9 to 12.9 GHz is achieved. Furthermore, two transmission zeros, namely, TZ_1 and TZ_2, on each side of passband are introduced by the capacitive source-load coupling, as shown in Figures 5(a) and (b), respectively.

After investigating the characteristics of the dual-mode filter with source-load coupling structure, a photograph of the fabricated filter is shown in Figure 6. The proposed filter is measured by use of an Agilent E5071C network analyzer, as shown in Figure 6(a). Figure 6(b) shows the simulation and measurement results. The measured results show

that the passband is centered at 5.22 GHz with the 3 dB fractional bandwidth of 8.5% which is in good agreements with those of the simulation, and the insertion loss and return loss are 1.3 dB and 18.4 dB respectively. Measured results show that the proposed filter has two transmission zeros, namely, TZ_1 and TZ_2, which are located at 4.37 and 6.2 GHz with attenuations of 53.4 and 30.5 dB respectively.

3. DUAL-MODE DUAL-BAND BANDPASS FILTER WITH HIGH FREQUENCIES SELECTIVITY

The layout of the proposed dual-band bandpass filter with its two bands located at 3.4/4.5 GHz is shown in Figure 7(a). It consists of a pair of symmetrical TSLSIRs. The coupling scheme of proposed filter is shown in Figure 7(b). This structure has the advantage of that it may enable each passband to have high frequency selectivity. The final structure dimensions of the proposed filter are given in Table 2. The filter is also fabricated on the Rogers RT/Duroid5880 substrate with dielectric constant ratio ε_r of 2.2 and thickness h of 0.508 mm.
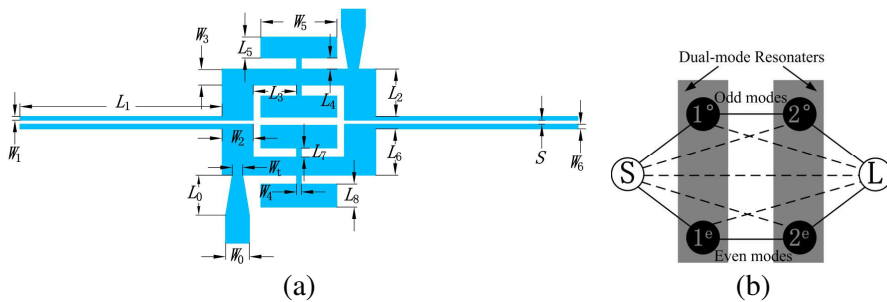
Figure 7. (a) The layout of the proposed dual-mode dual-band bandpass filter. (b) The coupling scheme for the proposed filter.

3.1. Analysis of Dual-mode Symmetrical TSLSIR with Open-circuited Loaded Case

The proposed dual-mode symmetrical TSLSIR with open-circuited loaded case is illustrated in Figure 8(a). Because the dual-mode resonator in Figure 8(a) is symmetrical about the A-A' plane, the odd- and even-mode theory may also be employed to analyze it. The odd-mode equivalent circuit of TSLSIR with open-circuited loaded case is

Table 2. Dimensions of the proposed dual-mode dual-band bandpass filter.

Parameters	Values	Parameters	Values	Parameters	Values
W_t	0.67	W_5	4.94	L_3	2.82
W_0	1.54	W_6	0.3	L_4	0.72
W_1	0.25	S	0.26	L_5	1.37
W_2	2.03	L_0	2.6	L_6	3.03
W_3	1.05	L_1	13.13	L_7	0.58
W_4	0.3	L_2	3.1	L_8	1.5
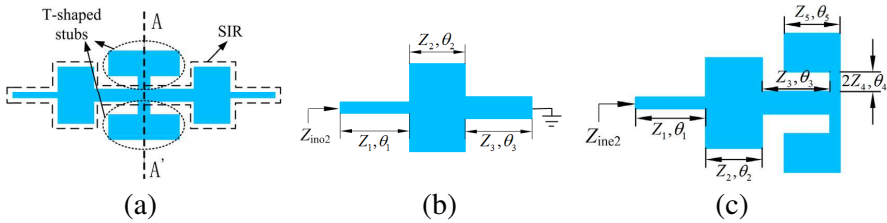
Figure 8. (a) Configuration of TSLSIR with open-circuited loaded case. (b) Odd mode equivalent circuits of TSLSIR. (c) Even-mode equivalent circuits of TSLSIR.

shown in Figure 8(b), and the input impedance may be expressed as:

$$Z_{\text{ino2}} = j \frac{\begin{aligned} &Z_1 Z_2^2 \tan\theta_2 + Z_1 Z_2 Z_3 \tan\theta_3 + Z_1^2 Z_2 \tan\theta_1 \\ &- Z_1^2 Z_3 \tan\theta_1 \tan\theta_2 \tan\theta_3 \end{aligned}}{\begin{aligned} &Z_1 Z_2 - Z_1 Z_3 \tan\theta_2 \tan\theta_3 - Z_2^2 \tan\theta_1 \tan\theta_2 \\ &- Z_2 Z_3 \tan\theta_1 \tan\theta_3 \end{aligned}} \quad (6)$$

Theoretically the resonance condition of odd mode is $Z_{\text{ino2}} = \infty$ and this implies:

$$Z_1 Z_2 - Z_1 Z_3 \tan\theta_2 \tan\theta_3 - Z_2^2 \tan\theta_1 \tan\theta_2 - Z_2 Z_3 \tan\theta_1 \tan\theta_3 = 0 \quad (7)$$

Similarly, for even-mode excitation of TSLSIR with open-circuited loaded case, the equivalent circuit is depicted in Figure 8(c), the even-mode resonance occurs when $Z_{\text{ine2}} = \infty$, and the Z_{ine2} may be

expressed as:

$$Z_{\text{ine2}} = j \frac{\begin{array}{l} Z_1(Z_2(Z_3(C+Z_3\tan\theta_3\cdot D)+Z_2\tan\theta_2(Z_3\cdot D-\tan\theta_3\cdot C)) \\ + Z_1\tan\theta_1(Z_2(Z_3(Z_3\cdot D-\tan\theta_3\cdot C)-\tan\theta_2 Z_3(C+Z_3\tan\theta_3\cdot D))) \end{array}}{\begin{array}{l} Z_1(Z_2(Z_3\cdot D-\tan\theta_3\cdot C)-Z_3\tan\theta_2(C+Z_3\tan\theta_3\cdot D)) \\ - Z_2\tan\theta_1(Z_3(C+Z_3\tan\theta_3\cdot D)+(Z_3\cdot D-\tan\theta_3\cdot C)Z_2\tan\theta_2) \end{array}} \quad (8)$$

where $C = Z_4(Z_4\tan\theta_4 - Z_5\cot\theta_5)$ and $D = Z_4 + Z_5\cot\theta_5\tan\theta_4$.

From Eqs. (7) and (8), it can be observed that the odd-mode resonant frequency depends on Z_1, Z_2, Z_3, θ_1, θ_2 and θ_3, and the even-mode resonant frequency depends on Z_1, Z_2, Z_3, Z_4, Z_5, θ_1, θ_2, θ_3, θ_4 and θ_5.

Figures 8(c) and 9(a) both are the even-mode equivalent circuits of TSLSIR with open-circuited loaded. In Figure 8(c), the length of the low impedance part of the stub is defined along horizontal orientation, whereas the low impedance part of the stub in Figure 9(a) is defined along vertical orientation. The calculated resonant frequencies may be obtained by substituting the parameters of the filter into the Eq. (8) and solving the equation by MATLAB program. The calculated frequencies results of the two models with different θ_5 are shown in Figure 9(b). For the equivalent circuit in Figure 8(c), when the value of θ_5 is 0.038 λ_g, i.e., 2.47 mm, the corresponding calculated frequency in Figure 9(b) is 4.71 GHz; for the equivalent circuit in Figure 9(a), when the value of θ_5 is 0.021λ_g, i.e., 1.37 mm, the corresponding calculated frequency is 4.78 GHz. The measured center frequency of the second passband of filter is 4.56 GHz. The relative frequency deviation of horizontal model in Figure 8(c) is 3.3%, and the relative frequency deviation of vertical model in Figure 9(a) is 4.8%. It can be seen

(a)   (b)
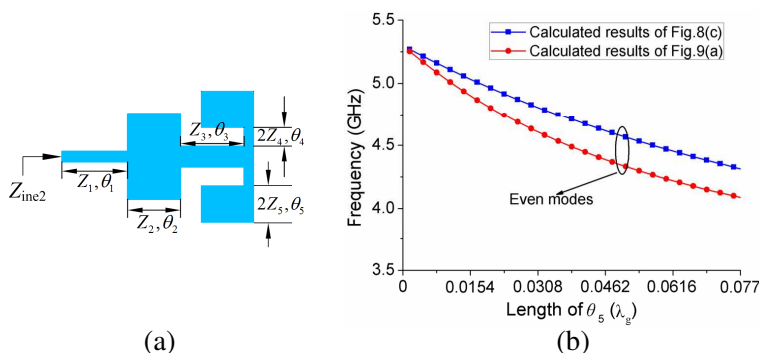
Figure 9. (a) The second even-mode equivalent circuits of TSLSIR with open-circuited loaded case. (b) The comparison between the results of Figures 8(c) and 9(a).

that the calculated frequency in Figure 8(c) is more accurate. So, the calculation of frequency should use the horizontal characteristic impedance and electrical length to ensure the accuracy of the even-mode equivalent circuit.

The calculated resonant frequencies may be obtained by substituting the parameters of the filter into the Eqs. (4), (7) and (8) and solving the equations by MATLAB program. The calculated resonant frequencies with different width parameters are shown in Figures 10(a) and (b). As shown in Figure 10(a), when W_1 and W_2 vary from 0.1 mm to 5 mm respectively, the odd mode resonant frequencies will decrease, but the odd mode resonant frequencies with different W_3 will grow. Meanwhile the even-mode resonant frequencies with different W_5 will decrease a little, and the frequencies with different W_4 will almost keep the same. The Figure 10(b) shows the calculated
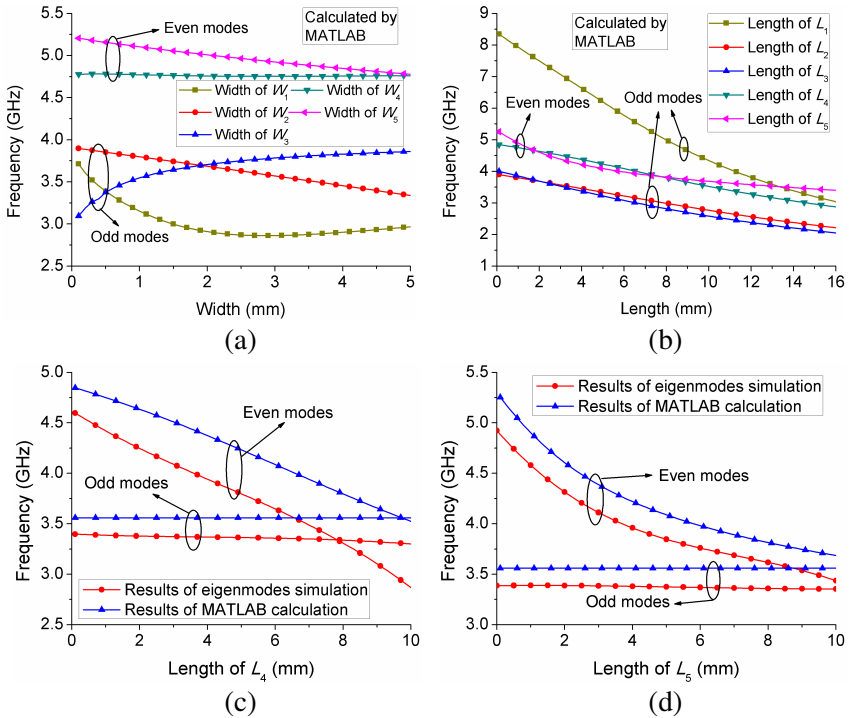
Figure 10. (a) The calculated resonant frequencies with varied width parameters. (b) The calculated resonant frequencies with varied length parameters. (c) The comparison between eigenmodes simulation and MATLAB calculation with the varied L_4. (d) The comparison between eigenmodes simulation and MATLAB calculation with the varied L_5.

resonant frequencies with different length parameters. As shown, when length parameters increase from 0.1 mm to 16 mm, the odd- and even-mode resonant frequencies will decrease almost linearly. Moreover it is can be observed that the impacting of the parameters of L_2 and L_3 on the odd mode resonant frequencies are almost the same and the same situation may also applies to the parameters of L_4 and L_5. So, based on the odd- and even-mode characteristics in Figures 10(a) and (b) it is easy to adjust the parameter to the desired responses during the design process.

Figure 10(c) shows the comparison between the results of eigenmodes simulation and those of MATLAB calculation with different L_4. It is observed that the calculated odd-mode frequency is about 3.56 GHz, the odd-mode frequency of eigenmodes simulation about 3.35 GHz, and the relative frequency deviation about 6.3%. Similarly, the frequency relative deviation between two even-mode curves in Figure 10(c) is about 10.3%. Figure 10(d) shows the comparison between the results of eigenmodes simulation and those of MATLAB calculation with different L_5. The relative frequency deviation between the two even-mode curves in Figure 10(d) is about 6.7%, and the relative frequency deviation between the two odd-mode curves is about 5.6%. It can be found that the results of MATLAB calculation agree well with those of eigenmodes simulation.

3.2. Dual-mode Dual-band Bandpass Filter Design

Figures 11(a) and (b) show the odd- and even-mode electric field patterns of the proposed filter, respectively. As shown in Figure 11(a), the electric field is dominant only in left- and right-branches, and this mode is an odd mode. Meanwhile, it can also be seen that the two symmetrical T-shaped loaded stubs do not affect the responses at the odd-mode resonant frequencies. On the other hand, the electric field in Figure 11(b) clearly shows that the electric field distributes in left- middle- and right-branches simultaneously and the electric field

(a)   (b)
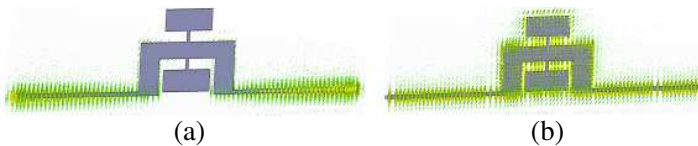
Figure 11. (a) Electric field pattern at the resonant frequency of odd mode. (b) Electric field pattern at the resonant frequency of even mode.

distribution is symmetric with respect to the middle-stub, therefore this resonance should be considered as an even-mode resonance.

Figure 12 shows the week coupling analysis of the proposed filter. In Figure 12(a), the even-mode frequency will move towards the lower frequency when L_4 increases, whereas the odd mode frequency will remain stationary. The same is true for Figure 12(b). It can be seen that the two even-mode resonant frequencies may be flexibly controlled by changing the length of L_4 or L_5, whereas the two odd modes resonant frequencies remain stationary.
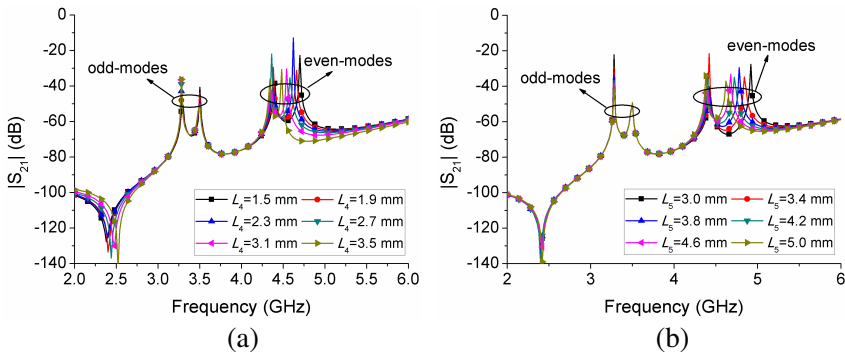
Figure 12. (a) The week coupling analysis with the varied L_4. (b) The week coupling analysis with the varied L_5.

Figure 13 shows the bandwidth characteristics of the proposed filter with different separation distances S. It may be seen that the coupling gap S can tune the bandwidths of the two passbands effectively, when S increased from $0.15\,\text{mm}$ to $0.3\,\text{mm}$, the bandwidth of the first passband decreases obviously, and the bandwidth of the second passband only changes a little. So, the desired bandwidth may be obtained by adjusting the coupling gap S, meanwhile the other performance is almost unaffected. Table 3 summarizes the fractional bandwidth of two passbands vs. different coupling gap S. In the Table 3, the FBW represents the simulated $3\,\text{dB}$ fractional bandwidth of passband.

Table 3. Simulated fractional bandwidth of two passbands vs. different S.

S	0.15	0.20	0.25	0.30
FBW of lower passband	13.2%	10.7%	8.7%	7.2%
FBW of upper passband	8.2%	7.9%	7.6%	7.1%
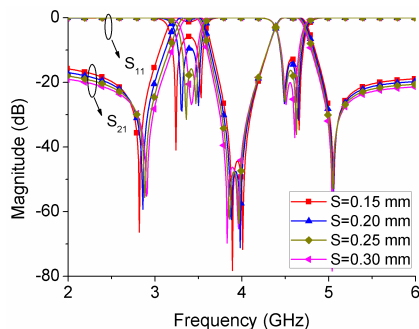
Figure 13. The analysis of the bandwidth with the varied S.

The coupling scheme of the proposed filter is shown in Figure 7(b). As shown in Figure 7(b), the emergence of the two passbands is due to the mutual coupling between the odd and even modes of the two dual-mode resonators, respectively. The two different coupling paths are independently controlled by odd and even modes, respectively. Because the taped feed line at the source side and the first resonator are an integrated structure, there should be a relative small coupling between the source and the second resonator. From this point, the source may be looked as directly coupling to the two modes of the second resonator [27]. The corresponding coupling path is shown in Figure 7(b) with dashed line. For the same principle, there should exist a weak coupling between the load and the first resonator, i.e., there should also be a directly coupling path between the load and the two modes of the first resonator. Finally, because of the use of tapped feed line and the integrated structure between the source/load and the first/second resonator respectively, it may be seen that there is also a weak coupling between the source and the load, and it is also indicated in Figure 7(b) with dashed line. Based on some previous work of filter synthesis[24, 27, 28], the coupling matrix of the proposed filter in Figure 7(b) is presented in Table 4, and the normalized frequency response of the coupling matrix is shown in Figure 14(a). Both frequency response curves of the simulation and coupling matrix are shown in Figure 14(b). It can be seen that the simulated results show good agreements with the responses of coupling matrix.

For this proposed filter, the two passbands are centered at 3.4 GHz and 4.54 GHz with the 3 dB fractional bandwidth of 8.4% and 7.5%, respectively. Meanwhile, four transmission zeros (TZ_1, TZ_2, TZ_3, TZ_4) are obtained at stopbands. Because these transmission zeros are quite close to the two passbands, very sharp increases of attenuations
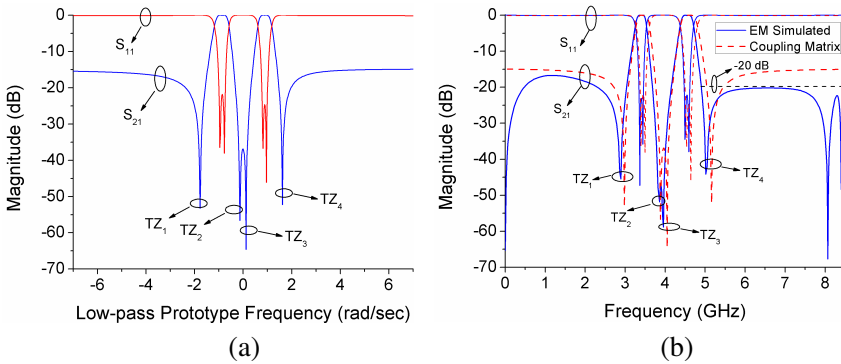
Figure 14. (a) Low-pass prototype frequency responses from coupling matrix. (b) Comparison of frequency response curves of the proposed filter.

Table 4. Coupling matrix for the filter.

	S	1°	2°	1^e	2^e	L
S	0	0.4353	0.0841	0.4361	−0.0183	−0.0904
1°	0.4353	0.8266	0.2189	0	0	−0.0344
2°	0.0841	0.2189	0.9474	0	0	0.4333
1^e	0.4361	0	0	−0.8913	0.2157	0.0131
2^e	−0.0183	0	0	0.2157	−0.9219	0.4276
L	−0.0904	−0.0344	0.4333	0.0131	0.4276	0

around the two passbands are observed. Between the two passbands there exists a high isolation characteristic with better than 47.4 dB suppression degrees in the range of 3.8 GHz to 3.98 GHz, at the same time the skirt selectivity between the two passbands is reasonably improved and the rejection of the spurious response from 4.9 GHz to 8.45 GHz is successfully suppressed to the level of lower than −20 dB. These properties should ensure good frequencies selectivity of the proposed filter.

The proposed filter is measured by use of an Agilent E5071C network analyzer and the photograph of filter measurement is shown in Figure 15(a). Figure 15(b) shows the simulation and measurement results with a photograph of the fabricated filter. The measured results show that two passbands are centered at 3.37 GHz and 4.56 GHz with the 3 dB fractional bandwidth of 5.9% and 6.5% respectively, and the insertion losses and return losses of two passbands are

1.81/22.6 dB and 1.53/20.4 dB respectively. Furthermore, the four transmission zeros (TZ$_1$, TZ$_2$, TZ$_3$, TZ$_4$) are located at 2.87 GHz, 3.8 GHz, 3.94 GHz and 5.04 GHz with attenuations of 56.7 dB, 46.6 dB, 63.3 dB and 43.8 dB, respectively. Meanwhile, a wide upper-stopband with harmonic suppression better than 20 dB in the range of 4.92 to 8.43 GHz is achieved. Figure 15(b) also provides a comparison of the measured and simulated characteristics of the filter, and an excellent agreement is observed.

(a)   (b)
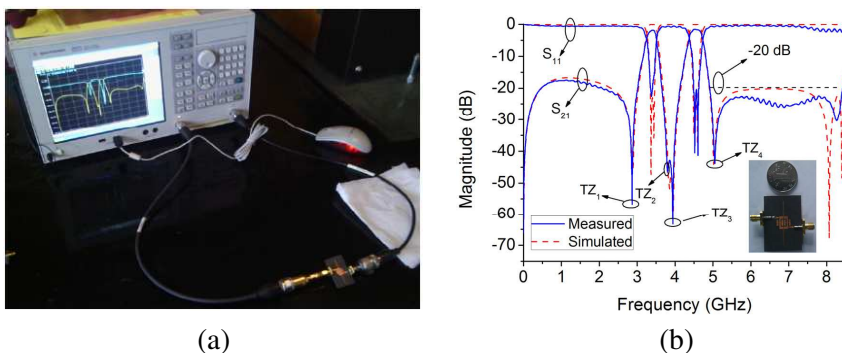
Figure 15. (a) The photograph of measured environment. (b) Simulation and measurement results with a photograph of fabricated filter.

3.3. Performance Comparisons

For comparison with the previous investigations, Table 5 summarizes the performance characteristics of some dual-mode dual-band bandpass filters, and it can be seen that the proposed dual-mode dual-band bandpass filter shows better relative upper-stopband bandwidth, high relative isolation bandwidth and good frequencies selectivity. In Table 5, F_{o1}, F_{o2}, IL, RL TZs, FS, IS and USB are the centre frequency of first passband, the centre frequency of second passband, the insertion loss of passband in dB, the return loss of passband in dB, the number of transmission zeros, the frequencies selectivity of four edges of the two passbands, the maximum isolation between two passbands, and the upper stopband bandwidth with 20 dB rejection. Furthermore, the 20 dB relative isolation bandwidth (RIB) between the two passbands is given by

$$\text{RIB} = \frac{20\,\text{dB isolation bandwidth}}{F_{o2} - F_{o1} - (BW_1/2 + BW_2/2)} \times 100\% \qquad (9)$$

Table 5. Measurement performances comparisons among published dual-mode dual-band bandpass filters and the proposed filter.

Ref.	F_{o1}/F_{o2} (GHz)	IL_1/RL_1	IL_2/RL_2	TZs	FS (dB/GHz)
[16]	2.4/5.7	1.2/17	0.8/20	3	108/264/14/25
[17]	2.4/5.16	0.6/28	1.4/12	4	127/156/194/200
[18]	2.3/4.8	1/17	1.8/17	2	18/131/13/15
[19]	1.36/1.9	0.6/13	1.3/15	2	31/75/184/143
[20]	2.46/5.2	0.4/17	0.5/15	3	120/59/24/87
[21]	5.15/7.3	2.8/20	2.5/20	4	69/60/50/49
This filter	3.37/4.56	1.8/22.6	1.5/20.4	4	128/141/131/120
Ref.	IS (dB)	20 dB RIB	20 dB RUSB	USB (GHz)	
[16]	40	23.4%	27.6%	1.9	
[17]	39.5	28.4%	1.4%	0.07	
[18]	17	0%	6.3%	0.42	
[19]	28.5	1.98%	7.6%	0.17	
[20]	39	24.4%	1.7%	0.12	
[21]	36.5	59.4%	0.94%	0.34	
This filter	63.3	48.7%	52.6%	3.51	

In Eq. (9), BW_1 and BW_2 are 3 dB bandwidth of the first and second passbands, respectively. The 20 dB relative upper-stopband bandwidth (RUSB) is also given by

$$\text{RUSB} = \frac{\text{upper stopband bandwidth}}{\text{centre frequency of upper-stopband}} \times 100\% \qquad (10)$$

4. CONCLUSIONS

In this paper, a novel approach for designing microstrip dual-mode bandpass filters based on symmetric TSLSIRs is proposed. Two prototype filters have been designed, fabricated and measured for experimental verification. The simulated and measured results show good agreements. Compared with the previous studies, the advantages of the proposed method not only achieve flexible designs for single or dual passband dual-mode filters, but also can obtain better

characteristics such as good relative upper-stopband bandwidth, high relative isolation bandwidth, increased number of transmission zeros and good frequencies selectivity.

ACKNOWLEDGMENT

REFERENCES

1. Karthikeyan, S. S. and R. S. Kshetrimayum, "Harmonic suppression of parallel coupled microstrip line bandpass filter using CSRR," *Progress In Electromagnetics Research Letters*, Vol. 7, 193–201, 2009.

2. Chin, K.-S. and D.-J. Chen, "Novel microstrip bandpass filters using direct-coupled triangular stepped-impedance resonators for spurious suppression," *Progress In Electromagnetics Research Letters*, Vol. 12, 11–20, 2009.

3. Liu, H.-W., L. Shen, Z.-C. Zhang, J.-S. Lim, and D. Ahn, "Dual-mode dual-band bandpass filter using defected ground waveguide," *Electronics Letters*, Vol. 46, No. 13, 895–897, 2010.

4. Chen, J. X., T. Y. Yum, J.-L. Li, and Q. Xue, "Dual-mode dual-band bandpass filter using stacked-loop structure," *IEEE Microwave and Wireless Components Letters*, Vol. 16, No. 9, 502–504, 2006.

5. Wang, J., L. Ge, K. Wang, and W. Wu, "Compact microstrip dual-mode dual-band bandpass filter with wide stopband," *Electronics Letters*, Vol. 47, No. 4, 263–265, 2011.

6. Hsu, C.-Y., C.-Y. Chen, and H.-R. Chuang, "A miniaturized dual-band bandpass filter using embedded resonators," *IEEE Microwave Wireless Components Letters*, Vol. 21, No. 12, 658–660, 2011.

7. Zheng, S.-Y. and W.-S. Chan, "Compact dual-band bandpass patch filter using coplanar waveguide feed method," *Electronics Letters*, Vol. 48, No. 23, 1475–1476, 2012.

8. Fu, S., B. Wu, J. Chen, S.-J. Sun, and C.-H. Liang, "Novel second-order dual-mode dual-band filters using capacitance loaded square

loop resonator," *IEEE Transactions on Microwave Theory and Techniques*, Vol. 60, 477–483, 2012.

9. Mashhadi, M. and N. Komjani, "Design of dual-band bandpass filter with wide upper stopband using SIR and GSIR structures," *Progress In Electromagnetics Research C*, Vol. 32, 221–232, 2012.

10. Mashhadi, M. and N. Komjani, "Design of novel dual-band bandpass filter with multi-spurious suppression for WLAN application," *Journal of Electromagnetic Waves and Applications*, Vol. 26, No. 7, 851–862, 2012.

11. Wolff, I., "Microstrip bandpass filter using degenerate modes of a microstrip ring resonator," *Electronics Letters*, Vol. 8, No. 12, 302–303, 1972.

12. Tan, B.-T., J.-J. Yu, S.-T. Chew, M.-S. Leong, and B.-L. Ooi, "A miniaturized dual-mode ring bandpass filter with a new perturbation," *IEEE Microwave and Wireless Components Letters*, Vol. 53, No. 1, 343–345, Jan. 2005.

13. Huang, X.-D. and C.-H. Cheng, "A novel coplanar-waveguide bandpass filter using a dual-mode square-ring resonator," *IEEE Microwave and Wireless Components Letters*, Vol. 16, No. 1, 13–15, Jan. 2006.

14. Kang, W., W. Hong, and J.-Y. Zhou, "Performance improvement and size reduction of microstrip dual-mode bandpass filter," *Electronics Letters*, Vol. 44, No. 6, 421–422, Mar. 2008.

15. Hong, J.-S., H. Shaman, and Y.-H. Chun, "Dual-mode microstrip open-loop resonators and filters," *IEEE Transactions on Microwave Theory and Techniques*, Vol. 55, No. 8, 1764–1770, Aug. 2007.

16. Lee, J. and Y. Lim, "Dual-band bandpass filter using dual-mode resonators," *Microwave and Optical Technology Letters*, Vol. 53, No. 11, 2515–2517, Nov. 2011.

17. Li, Y.-C., H. Wong, and Q. Xue, "Dual-mode dual-band bandpass filter based on a stub-loaded patch resonator," *IEEE Microwave and Wireless Components Letters*, 21, No. 10, 525–527, Oct. 2011.

18. Luo, S., L. Zhu, and S. Sun, "A dual-mode dual-band bandpass filter using a single ring resonator," *APMC: Asia Pacific Microwave Conference*, Vols. 1–5, 921–924, 2009.

19. Baik, J.-W., S. Pyo, W.-S. Yoon, and Y.-S. Kim, "Dual-mode dual-band bandpass filter for single substrate configuration," *Electronics Letters*, Vol. 45, No. 19, Sep. 2009.

20. Wu, X.-H., Q.-X. Chu, and X.-K. Tian, "Dual-band bandpass filter using novel side-stub-loaded resonator," *Microwave and*

Optical Technology Letters, Vol. 54, No. 2, 362–364, Feb. 2012.

21. Zhao, L.-P., X.-W. Dai, Z.-X. Chen, and C.-H. Liang, "Novel design of dual-mode dual-band bandpass filter with triangular resonators," *Progress In Electromagnetics Research*, Vol. 77, 417–424, 2007.

22. Athukorala, L. and D. Budimir, "Compact dual-mode open loop microstrip resonators and filters," *IEEE Microwave and Wireless Components Letters*, Vol. 19, No. 11, 698–670, 2009.

23. Liao, C.-K., P.-L. Chi, and C.-Y. Chang, "Microstrip realization of generalized Chebyshev filters with box-like coupling schemes," *IEEE Transactions on Microwave Theory and Techniques*, Vol. 55, No. 1, 147–153, Jan. 2007.

24. Cameron, R.-J., "Advanced coupling matrix synthesis techniques for microwave filters," *IEEE Transactions on Microwave Theory and Techniques*, Vol. 51, No. 1, 1–10, Jan. 2003.

25. Amari, S., U. Rosenberg, and J. Bornermann, "Adaptive synthesis and design of resonator filters with source/load-multiresonator coupling," *IEEE Transactions on Microwave Theory and Techniques*, Vol. 50, No. 8, 1969–1977, Aug. 2002.

26. Wang, J.-P., J.-L. Li, J. Ni, S.-S. Zhao, W. Wu, and D.-G. Fang, "Design of miniaturized microstrip dual-mode filter with source-load coupling," *IEEE Microwave Wireless Component Letters*, Vol. 20, No. 6, 319–321, 2010.

27. Wu, Y.-l., X.-M. Zhong, X.-Z. Xiong, and C. Liao, "Design of dual-mode dual-band bandpass filters with controllable frequencies for multimode wireless communication applications," *Journal of Electromagnetic Waves and Applications*, Vol. 27, No. 17, 2176–2189, 2013.

28. Kuo, Y.-T. and C.-Y. Chang, "Analytical design of two-mode dual-band filters using E-shaped resonators," *IEEE Transactions on Microwave Theory and Techniques*, Vol. 60, No. 2, 250–260, Feb. 2012.